RESEARCH ARTICLE

WILEY

Tracer-specific reference tissues selection improves detection of ^{18}F-FDG, ^{18}F-florbetapir, and ^{18}F-flortaucipir PET SUVR changes in Alzheimer's disease

Yanxiao Li[1,2] | Yee Ling Ng[1] | Manish D. Paranjpe[3] | Qi Ge[1] | Fengyun Gu[1,4] |
Panlong Li[5] | Shaozhen Yan[6] | Jie Lu[6] | Xiuying Wang[2] | Yun Zhou[1] |
for the Alzheimer's Disease Neuroimaging Initiative

[1]Central Research Institute, United Imaging Healthcare Group Co., Ltd, Shanghai, China

[2]School of Computer Science, The University of Sydney, Sydney, New South Wales, Australia

[3]Harvard-MIT Health Sciences and Technology Program, Harvard Medical School, Boston, Massachusetts, USA

[4]Department of Statistics, University College Cork, Cork, Ireland

[5]School of Electrical and Information Engineering, Zhengzhou University of Light Industry, Zhengzhou, Henan, China

[6]Department of Radiology and Nuclear Medicine, Xuanwu Hospital, Capital Medical University, Beijing, China

Correspondence
Yun Zhou, United Imaging Healthcare Group Co. Ltd, 2258 Chengbei Road, Jiading District, Shanghai 201807, China.
Email: yun.zhou@united-imaging.com

Xiuying Wang, School of Computer Science, The University of Sydney, City Road, Camperdown/Darlington NSW 2006, Australia.
Email: xiu.wang@sydney.edu.au

Abstract

This study sought to identify a reference tissue-based quantification approach for improving the statistical power in detecting changes in brain glucose metabolism, amyloid, and tau deposition in Alzheimer's disease studies. A total of 794, 906, and 903 scans were included for ^{18}F-FDG, ^{18}F-florbetapir, and ^{18}F-flortaucipir, respectively. Positron emission tomography (PET) and T1-weighted images of participants were collected from the Alzheimer's disease Neuroimaging Initiative database, followed by partial volume correction. The standardized uptake value ratios (SUVRs) calculated from the cerebellum gray matter, centrum semiovale, and pons were evaluated at both region of interest (ROI) and voxelwise levels. The statistical power of reference tissues in detecting longitudinal SUVR changes was assessed via paired t-test. In cross-sectional analysis, the impact of reference tissue-based SUVR differences between cognitively normal and cognitively impaired groups was evaluated by effect sizes Cohen's d and two sample t-test adjusted by age, sex, and education levels. The average ROI t values of pons were 86.62 and 38.40% higher than that of centrum semiovale and cerebellum gray matter in detecting glucose metabolism decreases, while the centrum semiovale reference tissue-based SUVR provided higher t values for the detection of amyloid and tau deposition increases. The three reference tissues generated comparable d images for ^{18}F-FDG, ^{18}F-florbetapir, and ^{18}F-flortaucipir and comparable t maps for ^{18}F-florbetapir and ^{18}F-flortaucipir, but pons-based t map showed superior performance in ^{18}F-FDG. In conclusion, the tracer-specific reference tissue improved the detection of ^{18}F-FDG, ^{18}F-florbetapir, and ^{18}F-flortaucipir PET SUVR changes, which helps the early diagnosis, monitoring of disease progression, and therapeutic response in Alzheimer's disease.

1 | INTRODUCTION

Alzheimer's disease (AD) is a progressive neurodegenerative disease associated with memory deficits and cognitive impairments, brain deposition of amyloid-β (Aβ) peptide plaques, neurofibrillary tangles composed of hyperphosphorylated tau (ptau) protein, and glucose hypometabolism (DeTure & Dickson, 2019; Serrano-Pozo, Frosch, Masliah, & Hyman, 2011; Uddin et al., 2018). The standardized assessment of pathological processes underlying AD can be accomplished by biomarker-evidenced amyloid, tau, and neurodegeneration (ATN) framework (Jack Jr et al., 2018). Positron emission tomography (PET) using radiolabeled ligands including ^{18}F-FDG, ^{18}F-florbetapir, and ^{18}F-flortaucipir has been widely used to assess neurodegeneration, deposition of Aβ fibrils, and tau for diagnosis and monitoring progression of AD. Standardized uptake value ratio (SUVR) relative to a reference tissue is commonly used for ATN PET quantification. Specifically, ^{18}F-FDG SUVR can be used to estimate the metabolic glucose uptake rate ratio (Y. Wu et al., 2012; Y. G. Wu, 2008), while the ^{18}F-florbetapir and ^{18}F-flortaucipir SUVRs can be used to approximate the tracer distribution volume ratio (DVR) of binding to Aβ and tau, respectively (Wong et al., 2010; Zhou et al., 2021; Zhou, Endres, Brašić, Huang, & Wong, 2003; Zhou, Sojkova, Resnick, & Wong, 2012).

Various reference tissues-based SUVRs have been used in previous AD studies, leading to different statistical power in PET assessments (Chen et al., 2015; Zhou et al., 2021). The pons reference region previously demonstrated the best preservation of glucose metabolism in AD and therefore was deemed as a reliable reference tissue for brain ^{18}F-FDG PET normalization (Minoshima, Frey, Foster, & Kuhl, 1995). Reference tissues including whole brain (Nugent et al., 2020), cerebellum gray matter (GM; Förster et al., 2012; Ossenkoppele et al., 2012), and pons (Alexander, Chen, Pietrini, Rapoport, & Reiman, 2002; Ortner et al., 2019; Schmidt et al., 2008) have been used to calculate ^{18}F-FDG PET SUVR in longitudinal AD studies. The effect of reference tissues including cerebellum GM, pons, and whole brain on ^{18}F-FDG PET SUVR have been also evaluated in cross-sectional (Minoshima et al., 1995; Yakushev et al., 2008) and longitudinal AD studies (Nugent et al., 2020; Verger, Doyen, Campion, & Guedj, 2021). Similarly, different reference tissues including cerebellar GM, centrum semiovale, pons, and corpus callosum have been used to quantify ^{18}F-florbetapir and ^{11}C-PIB amyloid PET (Blautzik et al., 2017; Chen et al., 2015; Chiao et al., 2019; Heeman et al., 2020; Shokouhi et al., 2016; Su et al., 2015; Wang et al., 2021; Xie et al., 2020) and ^{18}F-flortaucipir tau PET (Baker et al., 2017; Cho et al., 2020; Devous Sr. et al., 2018; Southekal et al., 2018; Zhao, Liu, Ha, Zhou, & Alzheimer's Disease Neuroimaging Initiative, 2019). The amyloid PET SUVRs calculated from different reference tissues were compared and evaluated by correlation analysis of SUVR versus cognitive assessment (Chen et al., 2015), test–retest analysis (Blautzik et al., 2017), and effect size for evaluation of the treatment response (Chiao et al., 2019). Our previous research has demonstrated that spatially constrained kinetic model with dual reference tissues comprising of cerebellum GM and centrum semiovale significantly improves quantification of relative perfusion and tau binding (Zhou et al., 2021). In previous longitudinal ^{18}F-FDG and ^{18}F-florbetapir PET studies, different reference tissues based SUVRs were compared, but the comparisons were limited to the region of interest (ROI) levels. Also, these previous studies focused ^{18}F-FDG PET in normal aging (Nugent et al., 2020; Verger et al., 2021) or amyloid treatment effects in mild cognitive impairment (MCI) and AD participants (Chen et al., 2015; Chiao et al., 2019). Moreover, for tau PET studies, to the best of our knowledge, there has been no evaluation for multiple reference tissues in longitudinal studies.

The selection of an appropriate reference tissue is reliant on multivariable factors and imperative aspects such as the studied population, study sample size, PET acquisition protocol, and the type of radiopharmaceutical used. The objective of this study is to improve statistical power for detecting ^{18}F-FDG, ^{18}F-florbetapir, and ^{18}F-flortaucipir PET SUVR changes in AD by selecting appropriate reference tissues. Using the AD Neuroimaging Initiative (ADNI), we performed longitudinal analysis on individuals with disease progression regardless of their disease stage, whether from cognitively normal (CN) to AD, MCI to AD, or CN to MCI. The impact of the reference tissue selection on discriminating between CN and cognitively impaired (CI) were also evaluated. This study is the most comprehensive comparative analysis of different reference tissues measured with multiple radiotracers to monitor the progression of AD. Our study may improve clinical staging diagnosis through quantitative PET which has important implications for biomarker-guided precision medicine.

2 | MATERIALS AND METHODS

2.1 | Participants

All ^{18}F-FDG, ^{18}F-florbetapir, and ^{18}F-flortaucipir PET and structural MRI data in this study were obtained from the AD Neuroimaging Initiative (ADNI) dataset (https://adni.loni.usc.edu). Informed written consent was obtained from all participants at each site. In total, we downloaded 794 ^{18}F-FDG-PET scans, 906 ^{18}F-florbetapir-PET scans, and 903 ^{18}F-flortaucipir-PET scans, which encompass 420, 434, and

666 participants, respectively. Demographics and clinical assessments including the Mini-Mental Status Examination (MMSE), Clinical Dementia Rating (CDR), and clinical diagnostic status of CN, MCI, and AD participants were also obtained.

2.2 | PET data acquisition and image preprocessing

Raw T1-weighted structural MRI and preprocessed ^{18}F-FDG, ^{18}F-florbetapir, and ^{18}F-flortaucipir PET images of each subject were downloaded from the ADNI database. The downloaded PET images were aligned, averaged, reoriented, and interpolated into a standard $160 \times 160 \times 96$ voxel image grid and smoothed with an 8 mm in full width at half maximum (FWHM) 3D Gaussian filter by the ADNI consortium with 1.5 mm cubic voxels. Further details of PET and T1-weighted MR acquisition protocols can be found at http://adni.loni.usc.edu/methods/pet-analysis-method/pet-analysis/ and http://adni.loni.usc.edu/methods/documents/mri-protocols/, respectively.

The PET and MRI data were further processed by partial volume correction (PVC) and spatial normalization, both using Statistical Parametric Mapping (SPM12, Wellcome Department of Imaging Neuroscience, Institute of Neurology, London, UK) in the MATLAB R2020b (The MathWorks Inc., Natick, MA) environment, as reported in our earlier studies (Paranjpe et al., 2019; Yan et al., 2020, 2021). PVC was performed to minimize the possibility of underestimation in PET images, especially for small brain regions such as amygdala and striatum. The reblurred Van Cittert iteration method was applied for PVC in individual PET images, where a 3D Gaussian Kernel of 8 mm FWHM was used as the spatial smoothing function with step length α of 1.5 (Tohka & Reilhac, 2008). All PET images were then coregistered to the individual's own structural MRI images, which were normalized to the standard Montreal Neurologic Institute (MNI) space using an MRI template (image volume: $121 \times 145 \times 121$, voxel size: $1.5 \times 1.5 \times 1.5$ mm in x, y, z). The median (interquartile range) of time intervals between PET and MRI are 28(49) days, 30(48) days, and 51(129.5) days for ^{18}F-FDG, ^{18}F-florbetapir, and ^{18}F-flortaucipir, respectively. The transformation parameters determined by MRI spatial normalization were then applied to the coregistered PET images for PET spatial normalization. SUVR images were calculated relative to the cerebellum GM (SUVR$_{Cereb\_GM}$), centrum semiovale (SUVR$_{CS}$), and pons (SUVR$_{Pons}$) reference tissues. The ROI SUVR values were calculated by applying ROIs on the SUVR images in the standard MNI space for minimizing variance related to the variability of ROI volume and shape in native space (Gottesman et al., 2017; Liu et al., 2019; Paranjpe et al., 2019; Tudorascu et al., 2018; Yan et al., 2021). A total of 18 ROIs including three reference tissues (cerebellum GM, centrum semiovale, and pons) and an additional 15 ROIs including the orbital frontal, prefrontal, superior frontal, medial temporal, inferior temporal, lateral temporal, parietal, posterior precuneus, anterior cingulate, posterior cingulate, occipital, entorhinal cortex, amygdala, hippocampus, and parahippocampal gyrus regions were manually delineated on the MRI template using the PMOD software program (PMOD 4.002, PMOD Technologies Ltd., Zürich, Switzerland) in standard MNI space. These ROI templates were previously developed in the Johns Hopkins Department of Radiology and have been validated in our former studies (Liu et al., 2019; Paranjpe et al., 2019; Yan et al., 2020, 2021; Zhou et al., 2021).

2.3 | Longitudinal SUVR PET analysis for cognitively declined participants

The effects of different reference tissues were evaluated on the sensitivity of SUVR measurements for the detection of cognitively declined populations. The baseline and last scans were defined as the subject's first and last scan in the downloaded data. Participants at the last scan who had an increased CDR score (Morris, 1993) or evidence of clinical disease progression (CN to MCI, MCI to AD, or CN to AD) were included in the longitudinal studies. This population inclusion criterion was consistent across ^{18}F-FDG, ^{18}F-florbetapir, and ^{18}F-flortaucipir studies. Based on the baseline and last scan SUVR values of each subject, paired statistical t values were calculated at both ROI- and voxel-levels for each reference tissue. The annual change rates for ^{18}F-FDG, ^{18}F-florbetapir, and ^{18}F-flortaucipir uptake were further calculated as follows:

$$\text{Annual Change Rate } (ACR_x) \\ = (SUVR_{last\ scan} - SUVR_{baseline})/(SUVR_{baseline} * T), \quad (1)$$

where x represents the reference tissue (cerebellum GM, centrum semiovale, or pons), SUVR$_{last\ scan}$ and SUVR$_{baseline}$ are the SUVR values of the ROI at the last scan and baseline, T is the time interval from baseline to the last scan in years.

2.4 | Cross-sectional SUVR PET analysis for CN and CI participants

To comprehensively assess the performance of the cerebellum GM, centrum semiovale, and pons reference tissues in discriminating between CN or CI individuals, ROI- and voxelwise-based cross-sectional statistical analyses were performed. All baseline scans were included for cross-sectional analysis and participants were classified as either CN (CDR = 0) or CI (CDR ≥ 0.5; Zhou et al., 2021). To investigate the sensitivity of the PET SUVR measurement in discriminating CN from CI, effects sizes were approximated using Cohen's d (Chand et al., 2020; Cohen, 1988; Lopresti et al., 2005; Sullivan & Feinn, 2012; Zhou et al., 2021) of CN and CI groups as follows:

$$d = (\text{mean}(SUVR_x \text{ at group } 1) - \text{mean}(SUVR_x \text{ at group } 2)) - SD_{pooled}, \quad (2)$$

where SD_{pooled} represents the standard deviation of SUVR in pooled population, x represents either cerebellum GM, centrum semiovale, or pons reference tissues. Since the ^{18}F-FDG SUVR decreased while the ^{18}F-florbetapir and ^{18}F-flortaucipir SUVR increased with disease progression, we set group 1 to be CN and group 2 to be CI for ^{18}F-FDG,

and group1 to be CI and group2 to be CN for ^{18}F-florbetapir and ^{18}F-flortaucipir.

For correcting the influence of covariates, the two-sample independent t test adjusted by age, sex, and education levels were performed at voxelwise level using SPM12. For ROI-based analysis, the generalized linear model was used to assess the group difference in SUVR for each ROI by adjusting for covariates, the Bonferroni-corrected p-value < .05 was defined as significant.

3 | RESULTS

3.1 | Study cohort characteristics

Study cohort characteristics for participants in the longitudinal analyses are summarized in Table 1. A total of 53, 55, and 20 participants were included with a mean time interval between the baseline and last scan of 63.42 ± 27.15 months, 57.05 ± 18.75 months, and 19.88 ± 8.03 months for ^{18}F-FDG, ^{18}F-florbetapir, and ^{18}F-flortaucipir, respectively. For each tracer, there were substantial differences between the baseline and last scan in age, education level, and CDR. There was no significant difference in the baseline and last scan for the MMSE of the participants in ^{18}F-flortaucipir. Comparison across tracers demonstrated that MMSE values at the baseline showed differences between ^{18}F-FDG and ^{18}F-flortaucipir groups and between ^{18}F-florbetapir and ^{18}F-flortaucipir groups. Other groups showed no significant difference in age and CDR in all three tracers.

Study cohort characteristics for participants in the cross-sectional study are listed in Table 2. There were no significant differences between CN and CI groups in terms of their age and education level, but considerable differences were observed for the MMSE and CDR scores for ^{18}F-FDG and ^{18}F-florbetapir PET studies. Significant differences were detected in age, education level, MMSE, and CDR scores in ^{18}F-flortaucipir PET study.

3.2 | Effect of reference tissue selection on sensitivity to detect longitudinal PET SUVR changes in AD

3.2.1 | ^{18}F-FDG PET

The statistic t maps based on the ^{18}F-FDG SUVR images for three reference tissues are illustrated in Figure 1. It was evident that the t-values calculated from SUVR images were in the order of $t(SUVR_{Pons})$ > $t(SUVR_{Cereb\_GM})$ > $t(SUVR_{CS})$ in the frontal, temporal and parietal regions. ROI-based analysis showed consistent results as demonstrated in Figure 2. The $t(SUVR_{Pons})$ showed the greatest sensitivity in the orbital frontal, prefrontal, superior frontal, lateral temporal, inferior temporal, posterior precuneus, anterior cingulate, posterior cingulate, caudate, entorhinal cortex, amygdala, hippocampus, and parahippocampal gyrus, 86.62 ± 47.63% higher than the $t(SUVR_{CS})$ and 38.40 ± 29.13% higher than the $t(SUVR_{Cereb\_GM})$. In contrast,

TABLE 1 Characteristics of longitudinal study cohort

	Mean ± SD			p value		
	^{18}F-FDG	^{18}F-florbetapir	^{18}F-flortaucipir	^{18}F-FDG versus ^{18}F-florbetapir	^{18}F-FDG versus ^{18}F-flortaucipir	^{18}F-florbetapir versus ^{18}F-flortaucipir
Participant (CN/MCI/AD)	29/22/2	25/29/1	9/8/3			
Scans	106	110	40			
Sex (M/F)	24/29	25/30	9/11			
Education (years)	15.40 ± 2.66	15.40 ± 2.65	15.50 ± 2.56			
Age (years) Baseline	74.53 ± 5.65	73.98 ± 6.90	77.17 ± 7.89	.65	.12	.09
Last scan	79.82 ± 5.94†	78.73 ± 7.26†	78.83 ± 7.98†	.40	.56	.96
MMSE Baseline	28.13 ± 1.83	27.89 ± 1.74	26.45 ± 3.39	.48	.01**	.02*
Last scan	25.08 ± 4.51†	24.65 ± 5.25†	25.25 ± 4.63	.66	.15	.66
CDR Baseline	0.21 ± 0.25	0.26 ± 0.25	0.35 ± 0.37	.25	.06	.25
Last scan	0.67 ± 0.48†	0.78 ± 0.51†	0.70 ± 0.52†	.24	.82	0.54

Note: Significant differences between the baseline and last scan values using two-sample t-test are denoted as †. Significant differences between the ^{18}F-FDG and ^{18}F-florbetapir group, ^{18}F-FDG and ^{18}F-flortaucipir group, ^{18}F-florbetapir, and ^{18}F-flortaucipir group are denoted by *, **, and *** when p < .05, .01, and 0.001, respectively.

SUVR$_{CS}$ had the lowest sensitivity and failed to detect SUVR decrease in the orbital frontal, prefrontal, and amygdala ($t < 1.67$). Compared with the SUVR$_{CS}$, the SUVR$_{Cereb\_GM}$ detected changes in the orbital frontal and prefrontal. The ACRs of ROIs for each reference tissue are listed in Table 3. The pons demonstrated the largest ACR across all listed brain regions, with an average of 73.8 ± 42.4% and 92.2 ± 61.7% higher than the ACR$_{Cereb\_GM}$ and ACR$_{CS}$, respectively. Regardless of which reference tissue was used, the caudate, anterior cingulate, lateral temporal, parahippocampal gyrus, posterior cingulate, parietal, and entorhinal cortex showed the greatest longitudinal annual change rates of ^{18}F-FDG uptake with each having at least a 1% reduction (Table 3).

3.2.2 | ^{18}F-florbetapir PET

In contrast to the ^{18}F-FDG PET analysis where the SUVR$_{Pons}$ demonstrated the greatest sensitivity, the SUVR$_{CS}$ in ^{18}F-florbetapir was superior in detecting longitudinal amyloid depositions (Figure 3). As demonstrated in Figure 4, significant longitudinal differences in the orbital frontal, prefrontal, superior frontal, lateral temporal, inferior temporal, parietal, posterior precuneus, occipital, anterior cingulate, and posterior cingulate were detected using the centrum semiovale reference tissue. The t(SUVR$_{CS}$) was 27.12 ± 12.31% and 52.12 ± 23.78% higher than the t(SUVR$_{Cereb\_GM}$) and t(SUVR$_{Pons}$), respectively, which was consistent with the t map at the voxel-level. The cerebellum GM and pons demonstrated similar sensitivities in monitoring all regions, however, the use of these reference tissues was unable to detect changes in the anterior cingulate. The greatest amyloid ACR for disease-progressed participants was observed in the posterior cingulate (2.2%) when centrum semiovale was used as reference tissue (Table 3). The average of ACRs in all the studied brain regions was 1.2% using a cerebellum GM reference tissue (ACR$_{Cereb\_GM}$), 1.7% using a centrum semiovale reference tissue (ACR$_{CS}$), and 1.6% using the pons reference (ACR$_{Pons}$) tissue (Table 3). ACR$_{CS}$ was 10.2 ± 1.8% and 44.3 ± 10.1% greater than the ACR$_{Cereb\_GM}$ and ACR$_{Pons}$, respectively, highlighting the superiority of the centrum semiovale in detecting longitudinal amyloid changes.

3.2.3 | ^{18}F-flortaucipir PET

The ROI and voxelwise results for ^{18}F-flortaucipir are displayed in Figures 5 and 6, respectively. Centrum semiovale reference tissue could only identify longitudinal changes in known AD-sensitive regions including the superior frontal, lateral temporal, and inferior temporal. The t(SUVR$_{CS}$) ranged from 2.02 to 2.34, which was 8.46 and 15.42 times higher than the t(SUVR$_{Cereb\_GM}$) and t(SUVR$_{Pons}$), respectively (Figure 6). The ACRs of these significant brain regions using three reference tissues are also listed in Table 3. The ACRs of the superior frontal, lateral temporal, and inferior temporal demonstrated an average of 3.2% when using the centrum semiovale as the reference tissue, exceeding ACR$_{Cereb\_GM}$ (0.5%) and ACR$_{Pons}$ (0.8%) by 5.5 and 3.2 times, respectively.

TABLE 2 Characteristics of cross-sectional study cohort

Characteristics	^{18}F-FDG			^{18}F-florbetapir			^{18}F-flortaucipir		
	CN	CI (MCI/AD)	p value	CN	CI (MCI/AD)	p value	CN	CI (MCI/AD)	p value
Participants (n)	168	252(220/32)		257	177(162/15)		395	271(205/66)	
Sex (M/F)	74/94	151/101		104/153	106/71		104/153	162/109	
Age (years)	72.79 ± 6.14	71.76 ± 7.89	.16	72.28 ± 6.41	71.77 ± 7.71	.45	73.31 ± 7.08	75.78 ± 8.37	<.0001***
Education (years)	16.57 ± 2.61	16.24 ± 2.66	.21	16.63 ± 2.52	16.33 ± 2.66	.23	16.84 ± 2.32	16.08 ± 2.68	.0001**
MMSE score	29.13 ± 1.14	27.43 ± 2.58	<.0001***	29.13 ± 1.06	27.53 ± 2.76	<.0001***	29.08 ± 1.18	26.48 ± 3.70	<.0001***
CDR	0.00 ± 0.04	0.52 ± 0.14	<.0001***	0.00 ± 0.04	0.52 ± 0.13	<.0001***	0.02 ± 0.12	0.56 ± 0.35	<.0001***

Note: Significant differences between CN and CI groups are denoted by *, **, and *** indicating $p < .05$, .01, and .001, respectively.

3.3 | Effect of reference tissue selection on sensitivity to detect PET SUVR differences between CN and CI groups in cross-sectional study cohort

The Cohen's d maps (Figure 7) generated from the cerebellum GM, centrum semiovale, and pons reference tissue-based SUVR images were visually comparable. The average d-values over 15 ROIs for the
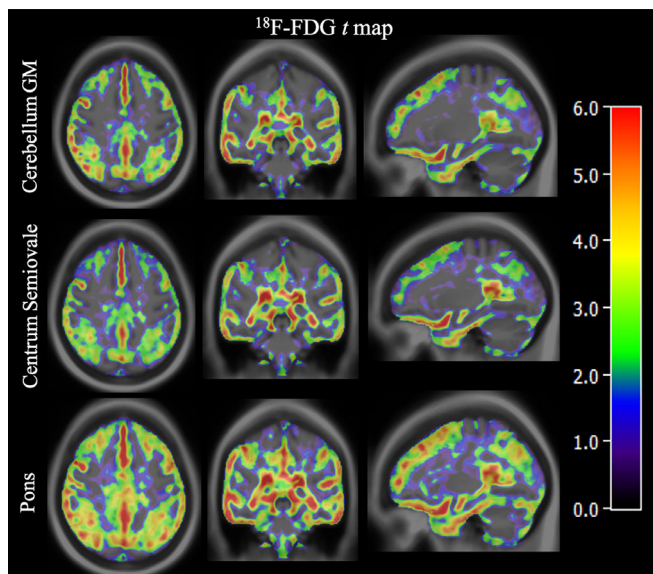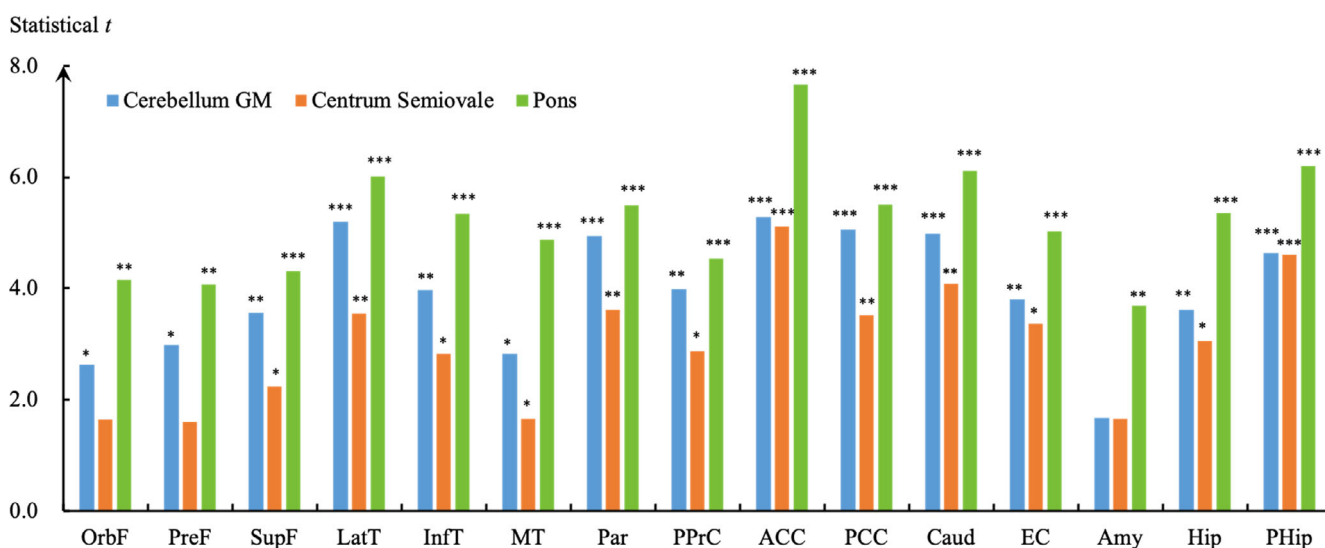
cerebellum GM, centrum semiovale and pons in ^{18}F-FDG were d(SUVR$_{Cereb\_GM}$) = 0.33 ± 0.89, d(SUVR$_{CS}$) = 0.30 ± 0.15 and d(SUVR$_{Pons}$) = 0.38 ± 0.35; in ^{18}F-florbetapir were d(SUVR$_{Cereb\_GM}$) = 0.44 ± 0.16, d(SUVR$_{CS}$) = 0.46 ± 0.14, and d(SUVR$_{Pons}$) = 0.49 ± 0.13; in ^{18}F-flortaucipir were d(SUVR$_{Cereb\_GM}$) = 0.60 ± 0.20, d(SUVR$_{CS}$) = 0.56 ± 0.23, and d(SUVR$_{Pons}$) = 0.59 ± 0.21. The covariates adjusted t maps (Figure 8) generated from reference tissue-based SUVR images were comparable in ^{18}F-florbetapir and ^{18}F-flortaucipir, but pons had increased performance in ^{18}F-FDG. The average t values from ROIs for the cerebellum GM, centrum semiovale, and pons in ^{18}F-FDG were t(SUVR$_{Cereb\_GM}$) = 3.52 ± 1.09, t(SUVR$_{CS}$) = 3.37 ± 0.96, and t(SUVR$_{Pons}$) = 4.76 ± 0.91; in ^{18}F-florbetapir were t(SUVR$_{Cereb\_GM}$) = 4.54 ± 1.67, t(SUVR$_{CS}$) = 4.75 ± 1.43, and t(SUVR$_{Pons}$) = 5.51 ± 1.20; in ^{18}F-flortaucipir were t(SUVR$_{Cereb\_GM}$) = 8.39 ± 2.58, t(SUVR$_{CS}$) = 7.51 ± 2.90, and t(SUVR$_{Pons}$) = 7.96 ± 2.67.

4 | DISCUSSION

In this study, we evaluated the effect of reference tissue selection on the statistical power to detect longitudinal and cross-sectional SUVR changes in ^{18}F-FDG, ^{18}F-florbetapir, and ^{18}F-flortaucipir PET studies of AD. Specifically, the results from ^{18}F-FDG were consistent with previous reference tissue selection studies in which the pons showed superiority in both longitudinal and cross-sectional analyses, especially in elucidating longitudinal SUVR changes (Minoshima et al., 1995; Nugent et al., 2020; Verger et al., 2021). After the correction of covariates (age, sex, and education level) effects in cross-sectional analysis, the pons demonstrated better performance in distinguishing

FIGURE 1 Paired statistical t map of longitudinal (mean follow-up period: 63.42 ± 27.15 months, n = 53) ^{18}F-FDG SUVR changes in participants with cognitive decline. The SUVR was calculated for reference tissue cerebellum GM, centrum semiovale, and pons, respectively

FIGURE 2 Statistical t values of ROI-based longitudinal ^{18}F-FDG SUVR changes in subjects with cognitive decline. Statistical p values indicate *p < .05, **p < .001, ***p < .0001. ACC, anterior cingulate; Amy, amygdala; Caud, Caudate; EC, entorhinal cortex; Hip, hippocampus; InfT, inferior temporal; LatT, lateral temporal; MT, medial temporal; OrbF, orbital frontal; Par, parietal; PCC, posterior cingulate; PHip, parahippocampal gyrus; PPrC, posterior precuneus; PreF, prefrontal; SupF, superior frontal

TABLE 3 Comparison of the annual change rates (%) of ^{18}F-FDG, ^{18}F-florbetapir, and ^{18}F-flortaucipir SUVR

		OrbF	PreF	SupF	LatT	MT	InfT	Par	PPrC	ACC	PCC	Caud	EC	Amy	Hip	PHiP	Occ
^{18}F-FDG	Cereb GM	−0.4 ± 2.8	−0.3 ± 2.6	−0.5 ± 2.6	−1.2 ± 2.6	−0.6 ± 2.4	−0.8 ± 2.4	−1.1 ± 2.6	−0.8 ± 2.7	−1.2 ± 2.9	−1.1 ± 2.6	−1.5 ± 3.0	−1.0 ± 3.2	−0.3 ± 2.9	−0.7 ± 2.4	−1.1 ± 3.0	−1.1 ± 2.3
	CS	−0.3 ± 3.3	−0.3 ± 3.5	−0.5 ± 3.3	−1.1 ± 3.3	−0.6 ± 2.8	−0.8 ± 2.6	−1.0 ± 3.0	−0.8 ± 3.3	−1.2 ± 2.6	−1.0 ± 3.2	−1.4 ± 3.4	−1.0 ± 2.9	−0.3 ± 2.9	−0.7 ± 2.6	−1.1 ± 2.4	−1.1 ± 2.4
	Pons	−0.9 ± 2.2	−0.8 ± 2.2	−1.0 ± 2.4	−1.7 ± 2.5	−1.1 ± 2.1	−1.3 ± 2.2	−1.5 ± 2.5	−1.3 ± 2.7	−1.7 ± 1.7	−1.6 ± 2.3	−2.0 ± 2.2	−1.5 ± 3.0	−0.8 ± 2.5	−1.2 ± 2.3	−1.6 ± 2.4	−1.6 ± 2.4
^{18}F-florbetapir	Cereb GM	1.3 ± 2.7	1.4 ± 2.4	1.3 ± 2.5	1.0 ± 2.0		0.8 ± 2.2	1.2 ± 2.2	1.3 ± 2.1	1.0 ± 3.0	1.8 ± 2.5						1.1 ± 2.3
	CS	1.8 ± 2.9	1.9 ± 2.4	1.8 ± 2.3	1.5 ± 2.2		1.3 ± 2.1	1.7 ± 2.1	1.8 ± 2.1	1.6 ± 3.6	2.4 ± 2.9						1.5 ± 1.9
	Pons	1.6 ± 2.7	1.7 ± 2.4	1.6 ± 2.4	1.4 ± 2.2		1.2 ± 2.2	1.5 ± 2.3	1.6 ± 2.2	1.4 ± 3.6	2.2 ± 2.9						1.4 ± 2.2
^{18}F-flortaucipir	Cereb GM			0.5 ± 3.1	0.5 ± 2.7		0.5 ± 3.1										
	CS			3.3 ± 6.4	3.2 ± 5.9		3.2 ± 5.7										
	Pons			0.8 ± 5.7	0.8 ± 4.8		0.7 ± 4.9										

*Note:* The values demonstrate ACRs of SUVRs in ^{18}F-FDG, ^{18}F-florbetapir and ^{18}F-flortaucipir when using the cerebellum GM, centrum semiovale, and pons as reference tissues.

Abbreviations: ACC, anterior cingulate; Amy, amygdala; Caud, Caudate; EC, entorhinal cortex; Hip, hippocampus; InfT, inferior temporal; LatT, lateral temporal; MT, medial temporal; Occ, Occipital; OrbF, orbital frontal; Par, parietal; PCC, posterior cingulate; PHip, parahippocampal gyrus; PPC, posterior precuneus; PreF, prefrontal; SupF, superior frontal.

CN and CI groups, particularly in the orbital frontal, prefrontal, and inferior temporal (Table S1). Minoshima et al. (1995) evaluated pons and other reference tissues in AD by observing the preservation of glucose metabolism. They concluded that pons was a reliable and appropriate reference tissue for data normalization to distinguish between CN and CI groups. In the investigation of the metabolic changes of normal aging, pons was also identified as the most appropriate area for brain intensity normalization due to its minimal correlation with age and greater significant longitudinal cluster volumes compared to other normalizations (Verger et al., 2021). Similarly, in the context of healthy aging, pons was verified as the optimal reference tissue by examining changes in brain glucose uptake when comparing with the whole brain based on the posterior cingulate and the precuneus regions (Nugent et al., 2020). Although these previous studies have identified pons as the most appropriate reference tissue, these studies did not conduct voxelwise analysis and considered only a limited number of ROIs. More importantly, the longitudinal population these studies included were either normal aging or patients with only follow-up scans, regardless of the subjects' disease progression and clinical severity. In our study, we confirmed the use of pons in ^{18}F-FDG for the population with disease progression according to their clinical diagnosis. The annual reduction rates in ^{18}F-FDG uptake under normal aging in the anterior cingulate cortex and posterior cingulate cortex/precuneus were previously reported as 0.6 and 0.6% (Ishibashi et al., 2018). By using pons, our result illustrated that the ACRs of the subjects with clinical declines in the anterior cingulate and posterior cingulate were 1.7 and 1.6%, as more than twice as that of the normal participants reported (Ishibashi et al., 2018).

For ^{18}F-florbetapir amyloid PET, our results suggest that the centrum semiovale is the ideal reference tissue to detect ^{18}F-florbetapir longitudinal changes in AD for monitoring brain amyloid accumulation. The centrum semiovale showed the greatest statistical power to detect brain regions with highly significant t-values, as well as the highest ACR (ACR$_{CS}$ = 1.7%) compared to the cerebellum GM and pons. The cerebral white matter has been previously validated as the reference tissue with less variability and great statistical power to detect longitudinal increases in Aβ depositions (Chen et al., 2015). Interestingly, the application of subcortical white matter and cerebellar white matter alone or in combination produced an enhanced result when assessed by effect size (Cohen's d; Chiao et al., 2019). Moreover, in a test–retest ^{18}F-florbetapir longitudinal SUVR study, the brainstem had the highest stability and correlation between PET and concurrent cerebrospinal fluid Aβ$_{1−42}$ levels (Shokouhi et al., 2016). It is well-recognized that partial volume effects exist in brainstem- or pons-based SUVR measurements (Chen et al., 2015; Su et al., 2019). In our cross-sectional analysis including effect size estimates and two-independent sample t-test, cerebellum GM, centrum semiovale, and pons all demonstrated comparable statistical power in distinguishing SUVR differences between CN and CI groups. Cerebellum GM was ultimately recommended as the ideal reference tissue in ^{18}F-florbetapir PET studies especially in studies involving relative cerebellar perfusion measurement (Bilgel et al., 2020; Hsiao et al., 2013).

Our study also revealed the centrum semiovale as the optimal reference tissue for ^{18}F-flortaucipir tau PET studies. Superior frontal, lateral temporal, and inferior temporal were the only brain regions that were detected as significant using the centrum semiovale reference in tau PET. Considering the shorter time intervals between tau scans, all three reference tissues were indicated as the sensitive regions in tau PET imaging which strongly correlated with neurodegeneration (Zhou et al., 2021). To the best of our knowledge, this is the first study that
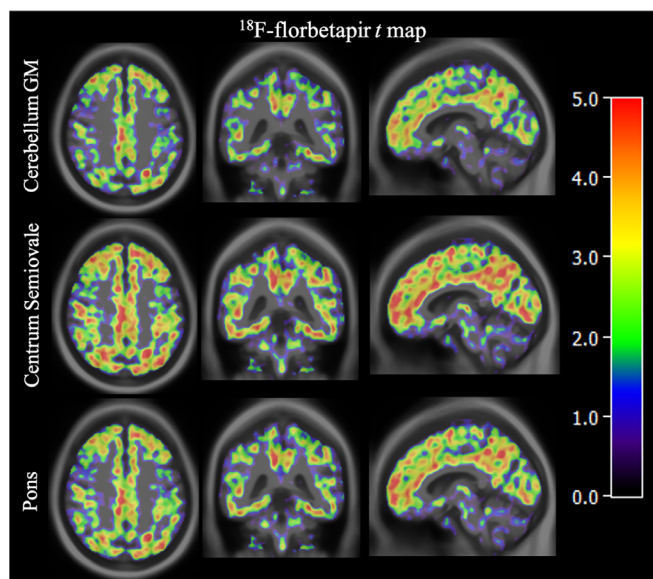
FIGURE 3 Paired statistical t map of longitudinal (mean follow-up period: 57.05 ± 18.75 months, $n = 55$) ^{18}F-florbetapir SUVR changes in participants with cognitive decline. The SUVR was calculated for reference tissue cerebellum GM, centrum semiovale, and pons, respectively

evaluated reference tissue effects longitudinally for tau PET. For cross-sectional analysis, the presented d maps and covariates adjusted t maps showed that the cerebellum GM, centrum semiovale, and pons revealed similar performance in ^{18}F-flortaucipir, but the cerebellum GM was still the recommended reference tissue due to previous cerebral blood flow studies (Rubinski et al., 2021; Zhou et al., 2021). Our previous research has demonstrated that the centrum semiovale reference tissue-based DVR and SUVR at the late phase, as well as the cerebellum GM reference tissue-based R_1 and SUVR at the early phase, demonstrated higher Cohen's d effect size to detect tau deposition with improved quantification power for dynamic ^{18}F-flortaucipir PET quantifications (Zhou et al., 2021). Notice that the cerebellum GM was frequently used as reference tissue in full dynamic ^{18}F-flortaucipir PET studies (Baker et al., 2017; Barret et al., 2017; Devous Sr. et al., 2018; Golla et al., 2017). The average ACR of tau obtained in this study when centrum semiovale as reference tissue was $ACR_{CS} = 3.22\%$, which was close to the previous annual ^{18}F-flortaucipir change of 4% collected from the inferior temporal region when cerebral white matter was used as the reference tissue (Hanseeuw et al., 2019).

To date, the cerebellum GM reference tissue, a region without relevant specific binding, has been suggested for the quantitation of amyloid and tau burden (Baker et al., 2017; Barret et al., 2017; Joachim, Morris, & Selkoe, 1989; Price et al., 2005; Yamaguchi, Hirai, Morimatsu, Shoji, & Nakazato, 1989), as well as for the quantification of the tracer perfusion (Bilgel et al., 2020; Weiner et al., 2013; Zhou et al., 2007, 2021). For example, cerebellum GM was the suggested reference tissue to estimate relative transport rate R_1 for dynamic ^{18}F-flortaucipir PET studies (Zhou et al., 2021). Based on the cerebellum GM reference, the R_1 images derived from ^{11}C-PIB dynamic PET have been used to assess the cerebral blood flow decreases in AD studies (Bilgel et al., 2020). Previous studies have also proposed and
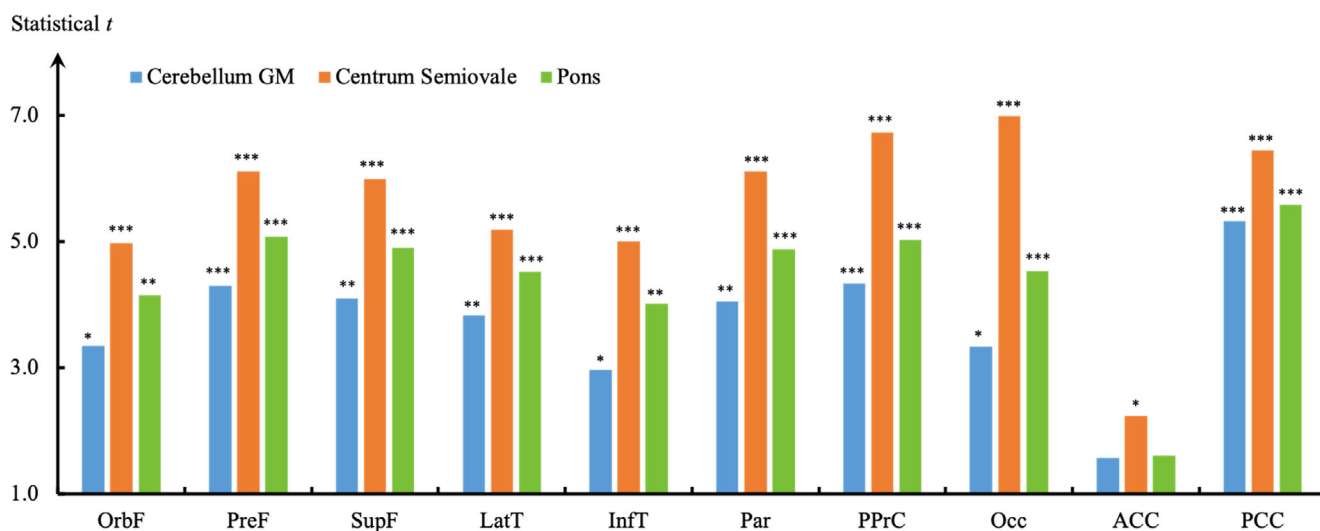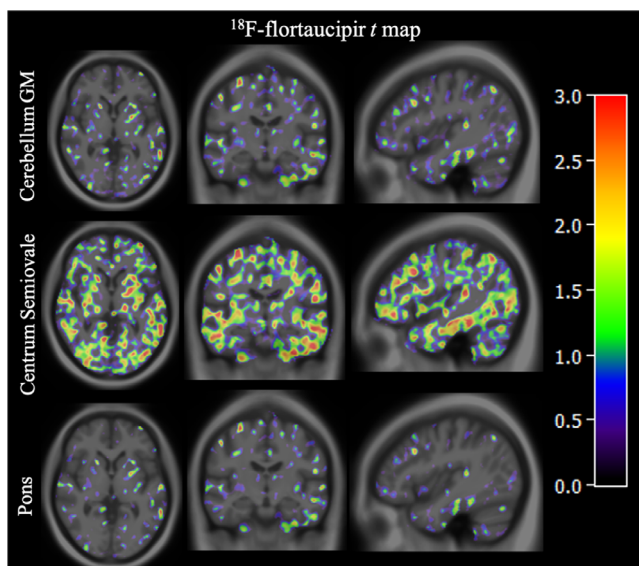

FIGURE 4 Statistical t values of ROI-based longitudinal ^{18}F-florbetapir SUVR changes in subjects with cognitive decline. Statistical p values indicate *$p < .05$, **$p < .001$, ***$p < .0001$. ACC, anterior cingulate; InfT, inferior temporal; LatT, lateral temporal; Occ, occipital; OrbF, orbital frontal; Par, parietal; PCC, posterior cingulate; PPrC, posterior precuneus; PreF, prefrontal; SupF, superior frontal

validated the benefits of using a white matter reference in longitudinal amyloid PET studies (Brendel et al., 2015; Chen et al., 2015). The cerebral white voxels were usually collected in the corpus callosum and centrum semiovale, rather than the cerebellum white matter which is close to gray matter or ventricles due to the likelihood of being confounded by the partial volume effect. Although the whole cerebellum is also used for cross-sectional analyses of florbetapir PET (Doraiswamy et al., 2012; Fleisher et al., 2013; Landau et al., 2013), a reference region including subcortical white matter is suggested for the measurement of the SUVR changes in longitudinal florbetapir PET study (Landau et al., 2015), which is consistent with our longitudinal study. We have also implemented the longitudinal analysis and

FIGURE 5 Paired statistical t map of longitudinal (mean follow-up period: 19.88 ± 8.03 months, $n = 20$) ^{18}F-flortaucipir SUVR changes in participants with cognitive decline. The SUVR was calculated for reference tissue cerebellum GM, centrum semiovale, and pons, respectively

covariates corrected cross-sectional analysis using the whole cerebellum (a combination of gray matter and white matter) reference tissue and compared the results. In the longitudinal analysis, the sensitivity of the whole cerebellum reference tissue to detect ^{18}F-FDG PET SUVR changes is lower than that of cerebellum GM and is close to that of white matter (centrum semiovale; Figure S1). In ^{18}F-florbetapir and ^{18}F-flortaucipir PET studies, the whole cerebellum still has comparable sensitivity to detect SUVR changes with centrum semiovale but has remarkable higher detection power as compared with cerebellum GM reference tissue (Figures S2 and S3). The covariates adjusted t-test showed that the whole cerebellum reference tissue based SUVR has the least sensitivity to discriminate CN and CI groups in both ^{18}F-FDG (Figure S4) and ^{18}F-florbetapir (Figure S4) when compared to the cerebellum GM, centrum semiovale and pons based SUVRs, specifically for the frontal and hippocampus (Table S1) in ^{18}F-FDG and occipital and parahippocampal gyrus in ^{18}F-florbetapir (Table S2). Whereas in ^{18}F-flortaucipir, the cerebellum GM, centrum semiovale, pons, and whole cerebellum demonstrate similar sensitivities in distinguishing CN and CI groups (Table S3 and Figure S4).

In conclusion, the reference tissue pons-based ^{18}F-FDG SUVR and centrum semiovale-based ^{18}F-florbetapir and ^{18}F-flortaucipir SUVR significantly improved the detection power of longitudinal PET changes in subjects with cognitive decline. For our cross-sectional analyses, the pons demonstrated a better performance in distinguishing CN and CI groups in ^{18}F-FDG. For amyloid and tau PET, the cerebellum GM, centrum semiovale and pons revealed a comparable statistical power to distinguish between CN and CI, but the cerebellum GM was suggested as the ideal reference tissue for quantification of relative cerebral blood flow, as well as amyloid and tau depositions using ^{18}F-florbetapir and ^{18}F-flortaucipir. The suggested tracer-specific reference tissues for SUVR calculation provide a basis for clinical quantitative ATN PET normalization and standardization. Our study supports an improved quantitative PET approach for early diagnosis, monitoring of disease progression, and therapeutic response in AD studies.
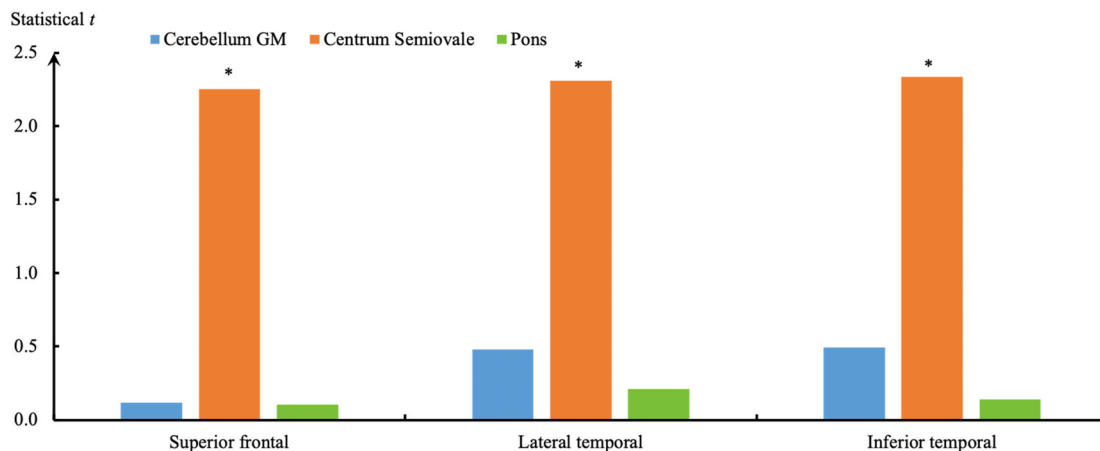

FIGURE 6 Statistical t values of ROI-based longitudinal ^{18}F-flortaucipir SUVR changes in subjects with cognitive decline. Statistical p values indicate *$p < .05$, **$p < .001$, ***$p < .0001$
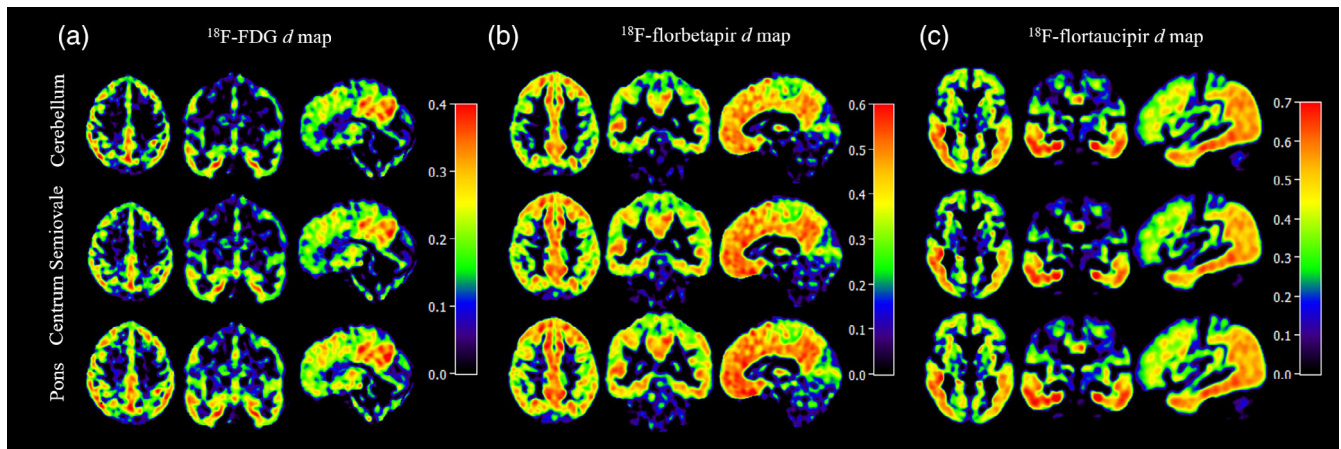
FIGURE 7 Statistical Cohen's *d* images for SUVR differences between cognitively normal (CN) and impaired (CI) groups in ^{18}F-FDG (a), ^{18}F-florbetapir (b), and ^{18}F-flortaucipir (c) PET studies when using cerebellum GM, centrum semiovale, and pons as reference tissue. The SUVR was calculated for reference tissue cerebellum GM, centrum semiovale, and pons, respectively
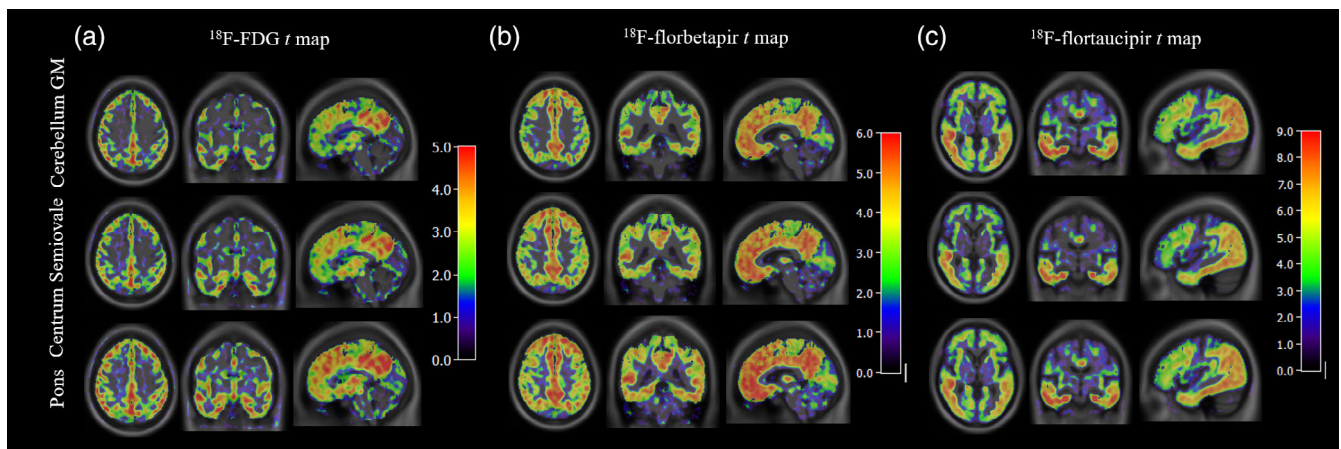
FIGURE 8 Statistical *t* images for SUVR differences between cognitively normal (CN) and impaired (CI) groups in ^{18}F-FDG (a), ^{18}F-florbetapir (b), and ^{18}F-flortaucipir (c) PET studies when using cerebellum GM, centrum semiovale, and pons as reference tissue. The SUVR was calculated for reference tissue cerebellum GM, centrum semiovale, and pons, respectively

DATA AVAILABILITY STATEMENT

All ^{18}F-FDG, ^{18}F-florbetapir, and ^{18}F-flortaucipir PET and structural MRI data in this study were obtained from the AD Neuroimaging Initiative (ADNI) dataset (https://adni.loni.usc.edu).

ORCID

Jie Lu 🔲 https://orcid.org/0000-0003-0425-3921
Xiuying Wang 🔲 https://orcid.org/0000-0001-7160-5929
Yun Zhou 🔲 https://orcid.org/0000-0001-9135-336X

REFERENCES

Alexander, G. E., Chen, K., Pietrini, P., Rapoport, S. I., & Reiman, E. M. (2002). Longitudinal PET evaluation of cerebral metabolic decline in dementia: A potential outcome measure in Alzheimer's disease treatment studies. *The American Journal of Psychiatry*, 159(5), 738–745. https://doi.org/10.1176/appi.ajp.159.5.738

Baker, S. L., Lockhart, S. N., Price, J. C., He, M., Huesman, R. H., Schonhaut, D., & Jagust, W. J. (2017). Reference tissue-based kinetic evaluation of 18F-AV-1451 for tau imaging. *Journal of Nuclear Medicine*, 58(2), 332–338.

Barret, O., Alagille, D., Sanabria, S., Comley, R. A., Weimer, R. M., Borroni, E., & Morley, T. (2017). Kinetic modeling of the tau PET tracer 18F-AV-1451 in human healthy volunteers and Alzheimer disease subjects. *Journal of Nuclear Medicine*, 58(7), 1124–1131.

Bilgel, M., Beason-Held, L., An, Y., Zhou, Y., Wong, D. F., & Resnick, S. M. (2020). Longitudinal evaluation of surrogates of regional cerebral blood flow computed from dynamic amyloid PET imaging. *Journal of Cerebral Blood Flow and Metabolism*, 40(2), 288–297. https://doi.org/10.1177/0271678X19830537

Blautzik, J., Brendel, M., Sauerbeck, J., Kotz, S., Scheiwein, F., Bartenstein, P., & Alzheimer's Disease Neuroimaging Initiative. (2017). Reference region selection and the association between the rate of amyloid accumulation over time and the baseline amyloid burden. *European Journal of Nuclear Medicine and Molecular Imaging*, 44(8), 1364–1374. https://doi.org/10.1007/s00259-017-3666-8

Brendel, M., Högenauer, M., Delker, A., Sauerbeck, J., Bartenstein, P., Seibyl, J., ... Alzheimer's Disease Neuroimaging Initiative. (2015). Improved longitudinal [18F]-AV45 amyloid PET by white matter reference and VOI-based partial volume effect correction. *NeuroImage*, 108, 450–459.

Chand, G. B., Dwyer, D. B., Erus, G., Sotiras, A., Varol, E., Srinivasan, D., & Dazzan, P. (2020). Two distinct neuroanatomical subtypes of schizophrenia revealed using machine learning. *Brain*, 143(3), 1027–1038.

Chen, K., Roontiva, A., Thiyyagura, P., Lee, W., Liu, X., Ayutyanont, N., & Alzheimer's Disease Neuroimaging Initiative. (2015). Improved power for characterizing longitudinal amyloid-beta PET changes and evaluating amyloid-modifying treatments with a cerebral white matter reference region. *Journal of Nuclear Medicine*, 56(4), 560–566. https://doi.org/10.2967/jnumed.114.149732

Chiao, P., Bedell, B. J., Avants, B., Zijdenbos, A. P., Grand'Maison, M., O'Neill, P., & Koeppe, R. (2019). Impact of reference and target region selection on amyloid PET SUV ratios in the phase 1b PRIME study of Aducanumab. *Journal of Nuclear Medicine*, 60(1), 100–106. https://doi.org/10.2967/jnumed.118.209130

Cho, H., Baek, M. S., Lee, H. S., Lee, J. H., Ryu, Y. H., & Lyoo, C. H. (2020). Principal components of tau positron emission tomography and longitudinal tau accumulation in Alzheimer's disease. *Alzheimer's Research & Therapy*, 12(1), 114. https://doi.org/10.1186/s13195-020-00685-4

Cohen, J. (1988). *Statistical power analysis for the behavioral sciences* (2nd ed.). Hillsdale, NJ: Lawrence Erlbaum Associates Inc.

DeTure, M. A., & Dickson, D. W. (2019). The neuropathological diagnosis of Alzheimer's disease. *Molecular Neurodegeneration*, 14(1), 32. https://doi.org/10.1186/s13024-019-0333-5

Devous, M. D., Sr., Joshi, A. D., Navitsky, M., Southekal, S., Pontecorvo, M. J., Shen, H., & Mintun, M. A. (2018). Test-retest reproducibility for the tau PET imaging agent Flortaucipir F 18. *Journal of Nuclear Medicine*, 59(6), 937–943. https://doi.org/10.2967/jnumed.117.200691

Doraiswamy, P. M., Sperling, R. A., Coleman, R. E., Johnson, K. A., Reiman, E. M., Davis, M. D., & Fleisher, A. S. (2012). Amyloid-β assessed by florbetapir F 18 PET and 18-month cognitive decline: A multicenter study. *Neurology*, 79(16), 1636–1644.

Fleisher, A. S., Chen, K., Liu, X., Ayutyanont, N., Roontiva, A., Thiyyagura, P., & Sadowsky, C. H. (2013). Apolipoprotein E ε4 and age effects on florbetapir positron emission tomography in healthy aging and Alzheimer's disease. *Neurobiology of Aging*, 34(1), 1–12.

Förster, S., Yousefi, B. H., Wester, H.-J., Klupp, E., Rominger, A., Förstl, H., & Drzezga, A. (2012). Quantitative longitudinal interrelationships between brain metabolism and amyloid deposition during a 2-year follow-up in patients with early Alzheimer's disease. *European Journal of Nuclear Medicine and Molecular Imaging*, 39(12), 1927–1936.

Golla, S. S. V., Timmers, T., Ossenkoppele, R., Groot, C., Verfaillie, S., Scheltens, P., & Yaqub, M. (2017). Quantification of tau load using [(18)F]AV1451 PET. *Molecular Imaging and Biology*, 19(6), 963–971. https://doi.org/10.1007/s11307-017-1080-z

Gottesman, R. F., Schneider, A. L., Zhou, Y., Coresh, J., Green, E., Gupta, N., & Sharrett, A. R. (2017). Association between midlife vascular risk factors and estimated brain amyloid deposition. *JAMA*, 317(14), 1443–1450.

Hanseeuw, B. J., Betensky, R. A., Jacobs, H. I. L., Schultz, A. P., Sepulcre, J., Becker, J. A., & Johnson, K. (2019). Association of Amyloid and tau with COGNITION in preclinical Alzheimer disease: A longitudinal study. *JAMA Neurology*, 76(8), 915–924. https://doi.org/10.1001/jamaneurol.2019.1424

Heeman, F., Hendriks, J., Lopes Alves, I., Ossenkoppele, R., Tolboom, N., van Berckel, B. N. M., ... AMYPAD Consortium. (2020). [(11)C]PIB amyloid quantification: Effect of reference region selection. *EJNMMI Research*, 10(1), 123. https://doi.org/10.1186/s13550-020-00714-1

Hsiao, I. T., Huang, C. C., Hsieh, C. J., Wey, S. P., Kung, M. P., Yen, T. C., & Lin, K. J. (2013). Perfusion-like template and standardized normalization-based brain image analysis using 18F-florbetapir (AV-45/Amyvid) PET. *European Journal of Nuclear Medicine and Molecular Imaging*, 40(6), 908–920. https://doi.org/10.1007/s00259-013-2350-x

Ishibashi, K., Onishi, A., Fujiwara, Y., Oda, K., Ishiwata, K., & Ishii, K. (2018). Longitudinal effects of aging on (18)F-FDG distribution in cognitively normal elderly individuals. *Scientific Reports*, 8(1), 11557. https://doi.org/10.1038/s41598-018-29937-y

Jack, C. R., Jr., Bennett, D. A., Blennow, K., Carrillo, M. C., Dunn, B., Haeberlein, S. B., & Karlawish, J. (2018). NIA-AA research framework: Toward a biological definition of Alzheimer's disease. *Alzheimer's & Dementia*, 14(4), 535–562.

Joachim, C. L., Morris, J. H., & Selkoe, D. J. (1989). Diffuse senile plaques occur commonly in the cerebellum in Alzheimer's disease. *The American Journal of Pathology*, 135(2), 309.

Landau, S. M., Breault, C., Joshi, A. D., Pontecorvo, M., Mathis, C. A., Jagust, W. J., & Mintun, M. A. (2013). Amyloid-β imaging with Pittsburgh compound B and florbetapir: Comparing radiotracers and quantification methods. *Journal of Nuclear Medicine*, 54(1), 70–77.

Landau, S. M., Fero, A., Baker, S. L., Koeppe, R., Mintun, M., Chen, K., & Jagust, W. J. (2015). Measurement of longitudinal β-amyloid change with 18F-florbetapir PET and standardized uptake value ratios. *Journal of Nuclear Medicine*, 56(4), 567–574.

Liu, M., Paranjpe, M. D., Zhou, X., Duy, P. Q., Goyal, M. S., Benzinger, T. L. S., & Zhou, Y. (2019). Sex modulates the ApoE epsilon4 effect on brain tau deposition measured by (18)F-AV-1451 PET in individuals with mild cognitive impairment. *Theranostics*, 9(17), 4959–4970. https://doi.org/10.7150/thno.35366

Lopresti, B. J., Klunk, W. E., Mathis, C. A., Hoge, J. A., Ziolko, S. K., Lu, X., & DeKosky, S. T. (2005). Simplified quantification of Pittsburgh compound B amyloid imaging PET studies: A comparative analysis. *Journal of Nuclear Medicine*, 46(12), 1959–1972.

Minoshima, S., Frey, K. A., Foster, N. L., & Kuhl, D. E. (1995). Preserved pontine glucose metabolism in Alzheimer disease: A reference region for functional brain image (PET) analysis. *Journal of Computer Assisted Tomography*, 19(4), 541–547.

Morris, J. C. (1993). The clinical dementia rating (CDR): Current version and scoring rules. *Neurology*, 43(11), 2412–2414. https://doi.org/10.1212/wnl.43.11.2412-a

Nugent, S., Croteau, E., Potvin, O., Castellano, C. A., Dieumegarde, L., Cunnane, S. C., & Duchesne, S. (2020). Selection of the optimal intensity normalization region for FDG-PET studies of normal aging and Alzheimer's disease. *Scientific Reports*, 10(1), 9261. https://doi.org/10.1038/s41598-020-65957-3

Ortner, M., Drost, R., Hedderich, D., Goldhardt, O., Müller-Sarnowski, F., Diehl-Schmid, J., & Grimmer, T. (2019). Amyloid PET, FDG-PET or MRI? - the power of different imaging biomarkers to detect progression of early Alzheimer's disease. *BMC Neurology*, 19(1), 264. https://doi.org/10.1186/s12883-019-1498-9

Ossenkoppele, R., Tolboom, N., Foster-Dingley, J. C., Adriaanse, S. F., Boellaard, R., Yaqub, M., & van Berckel, B. N. (2012). Longitudinal imaging of Alzheimer pathology using [11C]PIB, [18F]FDDNP and [18F]FDG PET. *European Journal of Nuclear Medicine and Molecular Imaging*, 39(6), 990–1000. https://doi.org/10.1007/s00259-012-2102-3

Paranjpe, M. D., Chen, X., Liu, M., Paranjpe, I., Leal, J. P., Wang, R., & Zhou, Y. (2019). The effect of ApoE ε4 on longitudinal brain region-specific glucose metabolism in patients with mild cognitive impairment: A FDG-PET study. *NeuroImage: Clinical*, 22, 101795.

Price, J. C., Klunk, W. E., Lopresti, B. J., Lu, X., Hoge, J. A., Ziolko, S. K., & Mathis, C. A. (2005). Kinetic modeling of amyloid binding in humans using PET imaging and Pittsburgh compound-B. *Journal of Cerebral Blood Flow & Metabolism*, 25(11), 1528–1547.

Rubinski, A., Tosun, D., Franzmeier, N., Neitzel, J., Frontzkowski, L., Weiner, M., & Ewers, M. (2021). Lower cerebral perfusion is associated with tau-PET in the entorhinal cortex across the Alzheimer's continuum. *Neurobiology of Aging*, 102, 111–118. https://doi.org/10.1016/j.neurobiolaging.2021.02.003

Schmidt, R., Ropele, S., Pendl, B., Ofner, P., Enzinger, C., Schmidt, H., & Fazekas, F. (2008). Longitudinal multimodal imaging in mild to moderate Alzheimer disease: A pilot study with memantine. *Journal of Neurology, Neurosurgery, and Psychiatry*, 79(12), 1312–1317. https://doi.org/10.1136/jnnp.2007.141648

Serrano-Pozo, A., Frosch, M. P., Masliah, E., & Hyman, B. T. (2011). Neuropathological alterations in Alzheimer disease. *Cold Spring Harbor Perspectives in Medicine*, 1(1), a006189. https://doi.org/10.1101/cshperspect.a006189

Shokouhi, S., McKay, J. W., Baker, S. L., Kang, H., Brill, A. B., Gwirtsman, H. E., & Alzheimer's Disease Neuroimaging Initiative. (2016). Reference tissue normalization in longitudinal (18)F-florbetapir positron emission tomography of late mild cognitive impairment. *Alzheimer's Research & Therapy*, 8, 2. https://doi.org/10.1186/s13195-016-0172-3

Southekal, S., Devous, M. D., Sr., Kennedy, I., Navitsky, M., Lu, M., Joshi, A. D., & Mintun, M. A. (2018). Flortaucipir F 18 quantitation using parametric estimation of reference signal intensity. *Journal of Nuclear Medicine*, 59(6), 944–951. https://doi.org/10.2967/jnumed.117.200006

Su, Y., Blazey, T. M., Snyder, A. Z., Raichle, M. E., Marcus, D. S., Ances, B. M., & Benzinger, T. L. S. (2015). Partial volume correction in quantitative amyloid imaging. *NeuroImage*, 107, 55–64. https://doi.org/10.1016/j.neuroimage.2014.11.058

Su, Y., Flores, S., Wang, G., Hornbeck, R. C., Speidel, B., Joseph-Mathurin, N., & Benzinger, T. L. S. (2019). Comparison of Pittsburgh compound B and florbetapir in cross-sectional and longitudinal studies. *Alzheimers Dement (Amst)*, 11, 180–190. https://doi.org/10.1016/j.dadm.2018.12.008

Sullivan, G. M., & Feinn, R. (2012). Using effect size—Or why the P value is not enough. *Journal of Graduate Medical Education*, 4(3), 279–282.

Tohka, J., & Reilhac, A. (2008). Deconvolution-based partial volume correction in Raclopride-PET and Monte Carlo comparison to MR-based method. *NeuroImage*, 39(4), 1570–1584. https://doi.org/10.1016/j.neuroimage.2007.10.038

Tudorascu, D. L., Minhas, D. S., Lao, P. J., Betthauser, T. J., Yu, Z., Laymon, C. M., & Handen, B. L. (2018). The use of Centiloids for applying [11C] PiB classification cutoffs across region-of-interest delineation methods. *Alzheimer's & Dementia: Diagnosis, Assessment & Disease Monitoring*, 10(1), 332–339.

Uddin, M. S., Stachowiak, A., Mamun, A. A., Tzvetkov, N. T., Takeda, S., Atanasov, A. G., & Stankiewicz, A. M. (2018). Autophagy and Alzheimer's disease: From molecular mechanisms to therapeutic implications. *Frontiers in Aging Neuroscience*, 10, 4. https://doi.org/10.3389/fnagi.2018.00004

Verger, A., Doyen, M., Campion, J. Y., & Guedj, E. (2021). The pons as reference region for intensity normalization in semi-quantitative analysis of brain (18)FDG PET: Application to metabolic changes related to ageing in conventional and digital control databases. *EJNMMI Research*, 11(1), 31. https://doi.org/10.1186/s13550-021-00771-0

Wang, M., Yan, Z., Zhang, H., Lu, J., Li, L., Yu, J., & Jiang, J. (2021). Parametric estimation of reference signal intensity in the quantification of amyloid-beta deposition: An (18)F-AV-45 study. *Quantitative Imaging in Medicine and Surgery*, 11(1), 249–263. https://doi.org/10.21037/qims-20-110

Weiner, M. W., Veitch, D. P., Aisen, P. S., Beckett, L. A., Cairns, N. J., Green, R. C., & Liu, E. (2013). The Alzheimer's Disease Neuroimaging Initiative: A review of papers published since its inception. *Alzheimer's & Dementia*, 9(5), e111–e194.

Wong, D. F., Rosenberg, P. B., Zhou, Y., Kumar, A., Raymont, V., Ravert, H. T., & Pontecorvo, M. J. (2010). In vivo imaging of amyloid deposition in Alzheimer disease using the radioligand 18F-AV-45 (florbetapir [corrected] F 18). *Journal of Nuclear Medicine*, 51(6), 913–920. https://doi.org/10.2967/jnumed.109.069088

Wu, Y., Zhou, Y., Bao, S., Huang, S., Zhao, X., & Li, J. (2012). Using the rPatlak plot and dynamic FDG-PET to generate parametric images of relative local cerebral metabolic rate of glucose. *Chinese Science Bulletin*, 57(28–29), 3811–3818. https://doi.org/10.1007/s11434-012-5401-y

Wu, Y. G. (2008). Noninvasive quantification of local cerebral metabolic rate of glucose for clinical application using positron emission tomography and 18F-fluoro-2-deoxy-D-glucose. *Journal of Cerebral Blood Flow and Metabolism*, 28(2), 242–250. https://doi.org/10.1038/sj.jcbfm.9600535

Xie, Y., Yang, Q., Liu, C., Zhang, Q., Jiang, J., & Han, Y. (2020). Exploring the pattern associated with longitudinal changes of β-amyloid deposition during cognitively Normal healthy aging. *Front Med (Lausanne)*, 7, 617173. https://doi.org/10.3389/fmed.2020.617173

Yakushev, I., Landvogt, C., Buchholz, H. G., Fellgiebel, A., Hammers, A., Scheurich, A., & Bartenstein, P. (2008). Choice of reference area in studies of Alzheimer's disease using positron emission tomography with fluorodeoxyglucose-F18. *Psychiatry Research*, 164(2), 143–153. https://doi.org/10.1016/j.pscychresns.2007.11.004

Yamaguchi, H., Hirai, S., Morimatsu, M., Shoji, M., & Nakazato, Y. (1989). Diffuse type of senile plaques in the cerebellum of Alzheimer-type dementia demonstrated by β protein immunostain. *Acta Neuropathologica*, 77(3), 314–319.

Yan, S., Zheng, C., Paranjpe, M. D., Li, J., Benzinger, T. L. S., Lu, J., & Zhou, Y. (2020). Association of sex and APOE epsilon4 with brain tau deposition and atrophy in older adults with Alzheimer's disease. *Theranostics*, 10(23), 10563–10572. https://doi.org/10.7150/thno.48522

Yan, S., Zheng, C., Paranjpe, M. D., Li, Y., Li, W., Wang, X., & Alzheimer's Disease Neuroimaging Initiative. (2021). Sex modifies APOE epsilon4

dose effect on brain tau deposition in cognitively impaired individuals. *Brain*, *144*, 3201–3211. https://doi.org/10.1093/brain/awab160

Zhao, Q., Liu, M., Ha, L., Zhou, Y., & Alzheimer's Disease Neuroimaging Initiative. (2019). Quantitative (18)F-AV1451 brain tau PET imaging in cognitively normal older adults, mild cognitive impairment, and Alzheimer's disease patients. *Frontiers in Neurology*, *10*, 486. https://doi.org/10.3389/fneur.2019.00486

Zhou, Y., Endres, C. J., Brašić, J. R., Huang, S.-C., & Wong, D. F. (2003). Linear regression with spatial constraint to generate parametric images of ligand-receptor dynamic PET studies with a simplified reference tissue model. *NeuroImage*, *18*(4), 975–989. https://doi.org/10.1016/s1053-8119(03)00017-x

Zhou, Y., Flores, S., Mansor, S., Hornbeck, R. C., Tu, Z., Perlmutter, J. S., & Benzinger, T. L. S. (2021). Spatially constrained kinetic modeling with dual reference tissues improves (18)F-flortaucipir PET in studies of Alzheimer disease. *European Journal of Nuclear Medicine and Molecular Imaging*, *48*, 3172–3186. https://doi.org/10.1007/s00259-020-05134-w

Zhou, Y., Resnick, S. M., Ye, W., Fan, H., Holt, D. P., Klunk, W. E., & Wong, D. F. (2007). Using a reference tissue model with spatial constraint to quantify [11C] Pittsburgh compound B PET for early diagnosis of Alzheimer's disease. *NeuroImage*, *36*(2), 298–312.

Zhou, Y., Sojkova, J., Resnick, S. M., & Wong, D. F. (2012). Relative equilibrium plot improves graphical analysis and allows bias correction of standardized uptake value ratio in quantitative 11C-PiB PET studies. *Journal of Nuclear Medicine*, *53*(4), 622–628. https://doi.org/10.2967/jnumed.111.095927

SUPPORTING INFORMATION

Additional supporting information may be found in the online version of the article at the publisher's website.